

Deeply Learned Preselection of Higgs Dijet Decays at Future Lepton Colliders

So Chigusa^{1,2,3}, Shu Li^{4,5,6,7}, Yuichiro Nakai^{4,5}, Wenxing Zhang^{4,5}, Yufei Zhang^{4,5} and Jiaming Zheng^{5,4}

¹*Berkeley Center for Theoretical Physics, Department of Physics,
University of California, Berkeley, CA 94720, USA*

²*Theoretical Physics Group,
Lawrence Berkeley National Laboratory,
Berkeley, CA 94720, USA*

³*KEK Theory Center, IPNS, KEK,
Tsukuba, Ibaraki 305-0801, Japan*

⁴*Tsung-Dao Lee Institute,
Shanghai Jiao Tong University,
520 Shengrong Road, Shanghai 201210, China*

⁵*Institute of Nuclear and Particle Physics,
School of Physics and Astronomy,
Key Laboratory for Particle Physics and Cosmology,
Shanghai Jiao Tong University,
800 Dongchuan Road, Shanghai 200240, China*

⁶*Center for High Energy Physics, Peking University,
5 Yiheyuan Road, Beijing 100871, China*

⁷*School of Mechanical and Electronic Engineering, Suzhou University,
Suzhou 234000, Anhui, China*

Future electron-positron colliders will play a leading role in the precision measurement of Higgs boson couplings which is one of the central interests in particle physics. Aiming at maximizing the performance to measure the Higgs couplings to the bottom, charm and strange quarks, we develop machine learning methods to improve the selection of events with a Higgs decaying to dijets. Our methods are based on the Boosted Decision Tree (BDT), Fully-Connected Neural Network (FCNN) and Convolutional Neural Network (CNN). We find that the BDT and FCNN algorithms outperform the conventional cut-based method. With our improved selection of Higgs decaying to dijet events using the FCNN, the charm quark signal strength is measured with a 16% error, which is roughly a factor of two better than the 34% precision obtained by the cut-based analysis. Also, the strange quark signal strength is constrained as $\mu_{ss} \lesssim 35$ at the 95% C.L. with the FCNN, which is to be compared with $\mu_{ss} \lesssim 70$ obtained by the cut-based method.

Introduction.— The discovery of the Higgs boson at the Large Hadron Collider (LHC) [1, 2] has largely advanced our understanding of the origin of elementary particle masses. At the same time, the Higgs boson poses major puzzles that must be addressed by physics beyond the Standard Model (SM). The flavor puzzle asks why the SM fermion masses are hierarchically scattered. This is just rephrased into the hierarchies of the Yukawa couplings of the fermions to the Higgs field in the SM. To address the puzzles and reach a deeper understanding of the origin of masses, the scrutiny of the nature of the Higgs boson is essential. The LHC experiment has been searching for Higgs interactions with SM particles. The results are summarized in terms of the signal strength defined as the ratio of the observed production cross section times branching ratio to that predicted by the SM. To measure or constrain the quark Yukawa interactions, the LHC has performed various searches such as direct searches for a Higgs boson decaying to a pair of quarks or with an associated photon. The current observation/constraint in-

dicates [3–7]

$$\begin{aligned} \text{ATLAS : } \mu_{bb} &= 1.02^{+0.12+0.14}_{-0.11-0.13}, \quad \mu_{cc} < 26, \\ \text{CMS : } \mu_{bb} &= 1.01 \pm 0.22, \quad \mu_{cc} < 70, \end{aligned} \quad (1)$$

for the decay modes $H \rightarrow b\bar{b}$ and $H \rightarrow c\bar{c}$, respectively. Regarding the Yukawa interactions of lighter quarks [8], the direct observation of a Higgs boson decay to such quarks is extremely challenging at the LHC. In fact, the strange quark Yukawa coupling is constrained by the exclusive $H \rightarrow \phi\gamma$ decay [9–11], which sets the limit [12]

$$\mu_{ss} \lesssim 7.2 \times 10^8, \quad (2)$$

assuming the SM expectation for the Higgs-photon interaction. Future electron-positron colliders such as the Circular Electron Positron Collider (CEPC) [13], Future Circular Collider in electron mode (FCC-ee) [14] and International Linear Collider (ILC) [15] have advantages over the LHC in terms of the low background and well-defined initial state and are expected to significantly improve the precision measurement of Higgs boson interactions. Then, it is of critical importance to maximize the

search power of future colliders to accelerate the discovery of Higgs decay modes inaccessible at the LHC and to find any small deviation from the SM prediction that gives direct evidence of new physics.

There are two major steps in the measurement of the quark Yukawa coupling via direct searches for a Higgs boson decaying into a pair of quarks: the preselection to separate Higgs decaying to dijet ($H \rightarrow jj$) events from all non- $H \rightarrow jj$ background events and the subsequent jet flavor tagging. Regarding jet flavor tagging, bottom and charm quark jets are tagged by identifying displaced charged track vertices [16, 17]. The strange jet tagging has been discussed in refs. [18, 19] for the LHC and in ref. [20] for future e^+e^- colliders. In addition, recently, applications of machine learning (ML) techniques, in particular deep learning, to jet flavor tagging have been under intense investigation (see ref. [21] and references therein), and the improvement of the tagging performance has been reported. For instance, the Convolutional Neural Network (CNN) has been used to analyze jet substructures and identify boosted Higgs production modes; the production of $t\bar{t}h$ has been studied with extreme gradient boosted trees and neural network models [22–24]. On the other hand, the preselection of $H \rightarrow jj$ events at future e^+e^- colliders was studied by using the conventional cut-based method [25]. In the work presented in the talk [26], the Boosted Decision Tree (BDT) was used for the preselection only after the cut-based selection. Considering the success of ML applications in the jet flavor tagging, it is natural to test various ML algorithms including deep learning to improve the preselection, aiming at maximizing the performance to measure the Higgs couplings to the bottom, charm and strange quarks.

In the present letter, we develop ML methods based on the BDT, Fully-Connected Neural Network (FCNN) and Convolutional Neural Network (CNN) with the aim to improve the preselection of $H \rightarrow jj$ events at future e^+e^- colliders. We find that the BDT and FCNN-based algorithms outperform the cut-based method and that combined with the BDT introduced in ref. [26]. The resulting sensitivity to the signal strength for each Higgs decay mode of $H \rightarrow b\bar{b}$, $H \rightarrow c\bar{c}$ or $H \rightarrow s\bar{s}$ is then studied.

Event generation.– In order to investigate the preselection performance, we assume an e^+e^- collider with unpolarized e^+e^- beams, the center-of-mass energy $\sqrt{s} = 250$ GeV and the integrated luminosity $\mathcal{L} = 250$ fb $^{-1}$. Our focus is on the signal process with the $\nu\bar{\nu}H(\rightarrow jj)$ final state, either through the Higgs-strahlung $e^+e^- \rightarrow ZH$ with $Z \rightarrow \nu\bar{\nu}$ or the WW fusion, which possesses the highest sensitivity to $H \rightarrow jj$ [13, 25–27]. The signal process is characterized by two hard jets and a large missing transverse energy (MET) corresponding to the sum of two neutrino transverse momenta. We include all Higgs decay channels when generating the Higgs events.

The preselection methods described below will mostly pick up $H \rightarrow jj$ events. The main background processes are $e^+e^- \rightarrow ZZ$ and W^+W^- , both of which result in jets + MET when one of the vector bosons decays leptonically and the other decays hadronically. The remaining background processes are $e^+e^- \rightarrow q\bar{q}$, $e^\pm\nu W^\mp$ and e^+e^-Z , whose cross sections are not negligible. The cross section and the corresponding number of events of each signal/background process are listed in Table I.

Our simulation uses MadGraph5_aMC@NLO v2.6 [28] for Monte Carlo sample generation of hard scattering processes, PYTHIA8.2 [29, 30] for parton showering and hadronization and DELPHES v3.4 [31] with FastJet v1.0 [32] for jet clustering and detector simulation, where the default card of the CEPC in DELPHES v3.4 and default settings in PYTHIA8 are used.

Cut-based method.– We perform a cut-based preselection of $H \rightarrow jj$ events to set a benchmark for comparison. We adopt the same cut variables and criteria as those used in ref. [25], which are summarized as follows:

- Missing mass M_{miss}

Since $e^+e^- \rightarrow ZH$ is the dominant signal process, we consider a cut that picks up most of ZH events while reducing background events. We then use the missing mass defined as

$$M_{\text{miss}} \equiv \sqrt{(\sqrt{s} - E_{\text{vis}})^2 - \not{P}_T^2}, \quad (3)$$

where E_{vis} is the total energy of visible particles in an event and \not{P}_T is the total missing transverse momentum. For the ZH channel, \not{P}_T is ideally equal to the transverse momentum of the Higgs boson and M_{miss} peaks at the Z boson mass. Thus, we require $80 \text{ GeV} \leq M_{\text{miss}} \leq 140 \text{ GeV}$ as our selection criteria.

- $P_{T/L}$, P_{max} , N_{chd}

To reduce the $q\bar{q}$ background, we utilize the total transverse/longitudinal momentum of visible particles $P_{T/L}$ and the maximum track momentum P_{max} in an event. We require $20 \text{ GeV} < P_T < 70 \text{ GeV}$, $|P_L| < 60 \text{ GeV}$ and $P_{\text{max}} < 30 \text{ GeV}$ as our criteria. On the other hand, to well reduce the leptonic ($l\bar{l}l\bar{l}$) background, we set a cut on the number of charged tracks, $N_{\text{chd}} > 10$.

- Y_{12} , Y_{23}

We apply the k_T algorithm for the jet clustering,¹

¹ we use the variables Y_{12} and Y_{23} to extract events with exactly two hard partons, which correspond to two quarks from the Higgs decay for the signal processes. To correctly count the number of hard partons, it is necessary to use the k_T clustering algorithm.

Process	Signal		Background				
	$HZ(\rightarrow \nu\bar{\nu})$	$\nu\bar{\nu}H$ (WW fusion)	ZZ	W^+W^-	$q\bar{q}$	$e^\pm\nu W^\mp$	e^+e^-Z
Cross section in pb	0.0469	0.00774	1.03	15.4	50.2	5.14	4.73
Number of events	11725	1942	257250	3.85×10^6	1.255×10^7	1.285×10^6	1.182×10^6

TABLE I. The cross section and number of events of each signal/background process for the e^+e^- collision with $\sqrt{s} = 250$ GeV and an integrated luminosity of $\mathcal{L} = 250 \text{ fb}^{-1}$.

Process	Signal		Background				
	$HZ(\rightarrow \nu\bar{\nu})$	$\nu\bar{\nu}H$ (WW fusion)	ZZ	W^+W^-	$q\bar{q}$	$e^\pm\nu W^\mp$	e^+e^-Z
Before cut	11725	1942	275250	3.85×10^6	1.255×10^7	1.285×10^6	1.1825×10^6
$80 \text{ GeV} < M_{\text{miss}} < 140 \text{ GeV}$	8854	1322	83565	409174	33876	242224	241020
$20 \text{ GeV} < P_T < 70 \text{ GeV}$	8161	1072	49099	291164	4376	169402	144559
$ P_L < 60 \text{ GeV}$	7967	969	16086	145018	4043	83310	38178
$N_{\text{chd}} \geq 10$	7772	946	14072	53070	4009	4478	0
$P_{\text{max}} < 30 \text{ GeV}$	6963	855	10951	27265	2619	447	0
$Y_{23} < 0.02$	4623	554	7546	4344	2193	109	0
$0.2 < Y_{12} < 0.8$	4535	500	4995	3385	2008	91	0
$100 \text{ GeV} < M_{jj} < 130 \text{ GeV}$	4331	475	856	1677	277	50	0

TABLE II. The cut-flow of the preselection using the variables presented in the main text.

which defines the following variables [33–36]:

$$y_{ij} = \frac{2 \min(E_i^2, E_j^2)(1 - \cos \theta_{ij})}{E_{\text{vis}}^2}, \quad (4)$$

where $E_{i/j}$ denotes the energy of a (pseudo)particle labeled by i/j and θ_{ij} is the angle between the momenta of i and j . Two (pseudo)particles are clustered when the y -value satisfies $y_{ij} < y_{\text{cut}}$. Then, Y_{12} and Y_{23} are defined as the maximum and minimum values of y_{cut} with which an event contains exactly two jet in the final state, respectively. We require $Y_{23} < 0.02$ and $0.2 < Y_{12} < 0.8$ to further reduce background events mainly from the W^+W^- channel.

- Di-jet mass M_{jj}

We use the invariant mass of the two hardest jets in the final state M_{jj} , which is ideally equal to the Higgs mass for the signal events. Our requirement is $100 \text{ GeV} < M_{jj} < 130 \text{ GeV}$.

All of these variables are also used as inputs for the BDT and FCNN presented below.

Table II shows the cut-flow. Compared with ref. [25], we consider more general background processes including $e^+e^- \rightarrow e^\pm\nu W^\mp$ and $e^\pm e^\mp Z$. The main background events remaining after the cuts are $e^+e^- \rightarrow W^+W^-$ and ZZ . They could be further reduced by a harder cut on Y_{ij} . However, it also rejects a non-negligible fraction of signal events, which degrades the performance of the preselection.

BDT.— In order to take account of correlations among the variables listed in the cut-based method, we utilize a BDT algorithm whose inputs are those used in the cut-based method. The BDT is implemented with the

`scikit-learn` library [37], and its outputs are used as the unique variables for signal/background classification, or as a variable with which we further reduce background events on top of the cut-based preselection. The decision tree classifier has a maximum depth of 25 and requires a minimum of 30 samples for a leaf node. It is fitted by the AdaBoost-SAMME [38] algorithm with a learning rate of 0.1 and the maximum number of estimators is set to 75. These hyperparameters are manually chosen towards the best Higgs signal significance.

FCNN.— We implement the FCNN algorithm by using the `Keras 2.7.0` [39] application programming interface (API) with the `Tensorflow 2.7.0` [40] backend. We utilize a simple neural network in which every neuron in one layer connects to all neurons in the subsequent layer. In principle, this fully-connected neural network with a sufficient number of hidden layers has the ability to approximate any continuous function in a finite-dimensional space [41] and has a potential to learn features indistinguishable by the BDT. In our study, the variables used in the cut-based method are fed into the FCNN. We have tested various architectures and found that the best performance is achieved by a network with 9 hidden layers where the first 2 layers contain 100 neurons and the rest contain 90 neurons. We note that the performance of this network is only improved marginally beyond a smaller FCNN with 4 layers. We employ the Rectified Linear Unit (ReLU) as the activation function for the hidden layers and the softmax function for the output layer with two neurons. The optimizer is taken to be ADAM with the `Keras` default parameters and the loss function is cross entropy. The network outputs a score of the likelihood for an input event recognized as a $H \rightarrow jj$ signal event, which is used as the unique variable to classify signal/background events, or as a cut variable to reduce

Process	Signal		Background					Significance
	$HZ(\rightarrow \nu\bar{\nu})$	$\nu\bar{\nu}H$ (WW fusion)	W^+W^-	$q\bar{q}$	ZZ	$e^\pm\nu W^\mp$	e^+e^-Z	
Cut-based	4331	475	1677	277	856	50	0	54.9σ
BDT-only	6721	1047	61	195	399	9	0	84.6σ
FCNN-only	9562	1427	754	1101	419	109	1	95.0σ
CNN-only	4776	749	6337	5407	432	1237	552	39.6σ
Cut+BDT	3744	403	10	129	57	1	0	62.9σ
Cut+FCNN	3941	409	95	145	170	0	0	63.1σ
Cut+CNN	3733	409	289	219	486	0	0	57.8σ

TABLE III. The number of signal/background events and signal significance after each preselection method. BDT-only denotes the method that the output of the BDT is used as a unique variable to classify signal/background events. The same applies to FCNN-only and CNN-only. In Cut+BDT, the output of the BDT is used as a cut variable to reduce background events on top of the cut-based preselection. The same applies to Cut+FCNN and Cut+CNN.

background events on top of the cut-based preselection as in the case of the BDT.

CNN.– In addition to the BDT and FCNN, we test the CNN algorithm whose inputs are 2D event images. The image of an event has 3 “colors” [42]: particle momenta, particle charges and jet momenta. All the momenta are normalized by multiplying $1/\sqrt{s}$ for the stability of the network. 2D images are expanded in terms of the $\eta \times \phi$ coordinate system. The number of pixels for each channel is 33×36 where the size of a pixel is given by $\Delta\eta = 0.1(0.4)$ for $|\eta| < 1.0(1.0 < |\eta| < 3.4)$ and $\Delta\phi = 2\pi/36$. For the particle (jet) momentum color, a pixel value is defined as the vectorial summation of particle (jet) momenta inside the pixel, normalized by the collision energy. For the jet momentum color, the jet clustering is conducted by the anti- k_T algorithm [43]. We have also tested the b -tagging label as the fourth color but the performance is similar for 3 and 4 colors. The b -tagging pixel value is defined as the number of tight b -jets recognised by the anti- k_T algorithm. The CNN is implemented with the `TensorFlow` [40] framework and the `Keras` [39] API. The network architecture we utilize is summarized as follows. An input image with 3 or 4 colors for an event enters three convolutional layers each of which has 200 filters with 4×4 kernel. A max-pooling layer with 2×2 reduction follows. The generated feature maps are coupled to the fourth convolutional layer of 200 filters with 4×4 kernel. The 2D image is then flattened and coupled through fully-connected layers with 100, 100, 80, 80, 60 and 60 neurons respectively. The activation function is the ReLU for the hidden layers and the softmax function for the output layer with two neurons. The optimizer is Adadelata and the loss function is cross entropy. The optimizer is ADADELTA [44] with an initial learning rate of 0.3 and other parameters are set as the `Keras` default. As in the case of the BDT and FCNN, the network output is used as the unique variable to classify signal/background events, or as a cut variable on top of the cut-based selection.

Results.– Table III shows the number of signal (N_{sig}) and background (N_{bkg}) events remaining after each pre-

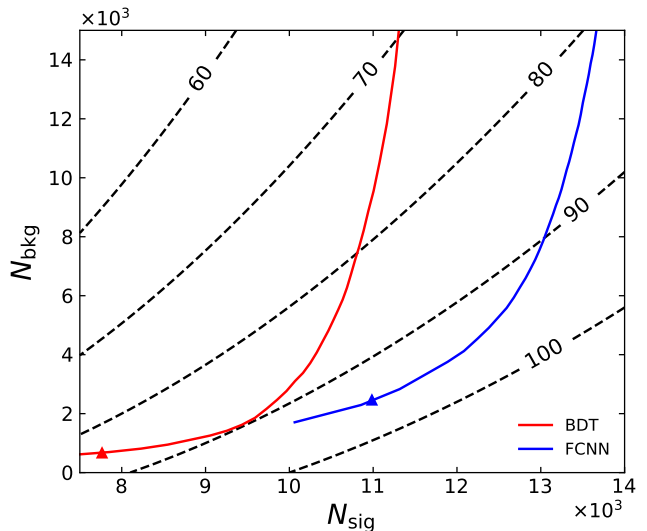


FIG. 1. The number of signal (N_{sig}) and background (N_{bkg}) events that passes the preselection using the BDT (red solid) and FCNN (blue solid). The triangle marker on the curve represents the number of events obtained by the classification threshold utilized in Table III. The black dashed curves denote contours of the signal significance.

selection method. We also estimate the signal significance $N_{\text{sig}}/\sqrt{N_{\text{bkg}} + N_{\text{sig}}}$ for comparison. The classification threshold of the BDT/FCNN/CNN output is chosen to obtain a large signal significance. The most suitable choice of the threshold depends on a physics variable that we would like to extract, e.g., the Yukawa coupling, because sensitivities to different variables are generally given by different combinations of N_{sig} and N_{bkg} .

We can see from Table III that the BDT-only method outperforms the cut-based method in terms of the signal significance, with more signal events and less background events after the preselection in each channel. We also find that the significance of the Cut+BDT method is worse than that of the BDT-only because the cut conditions are so strict that the number of signal events is excessively reduced. In fact, Table II shows that the significance could

	Cut-based	BDT-only	FCNN-only	Cut+BDT	Cut+FCNN
μ_{bb}	1 ± 0.021	1 ± 0.016	1 ± 0.013	1 ± 0.021	1 ± 0.021
μ_{cc}	1 ± 0.34	1 ± 0.16	1 ± 0.16	1 ± 0.21	1 ± 0.22
μ_{ss}	70	36	35	47	48

TABLE IV. The expected 1σ errors of the signal strength for the bottom (μ_{bb}) and charm (μ_{cc}) Yukawa couplings and the 95% C.L. upper limits on that of the strange quark (μ_{ss}) with various preselection methods presented in Table III, assuming statistical uncertainty only.

be no longer larger than 70σ after the cut-based preselection even if the BDT distinguished all background events from signal events. We note, however, that the presented signal significance does not faithfully reflect the performance of a specific application of the Higgs preselection such as the Yukawa coupling measurement.

The FCNN-only method shows the best signal significance among all preselection methods in Table III, which results from the highest signal acceptance and a high background rejection rate. The Cut+FCNN method is less efficient than the FCNN-only due to the similar reason discussed for the case of the BDT.

Figure 1 demonstrates the dependence of the BDT and FCNN results on the choice of the threshold. The relationship between N_{sig} and N_{bkg} for the BDT and FCNN analyses is plotted by scanning the threshold value. We can see that N_{sig} of the FCNN is larger than that of the BDT for any fixed value of N_{bkg} , indicating a clear advantage of the FCNN.

Most events that pass the preselection by the BDT or FCNN, regardless of being a true Higgs event or not, have di-jet masses within $120 \sim 125.2 \text{ GeV}$.² Furthermore, since the flavor information is not used in training, all quark flavors are equally likely to pass the preselection. Indeed, we have fed equal numbers of events from $h \rightarrow b\bar{b}$, $h \rightarrow c\bar{c}$ and $h \rightarrow g\bar{g}$ into the trained BDT and FCNN and observed almost equal passing rates. Therefore, the tested BDT and FCNN architectures mostly select $H \rightarrow q\bar{q}$ signals in a flavor-blind manner, which is crucial for measuring the quark Yukawa couplings.

The signal significance of the CNN-only method is observed to be much worse than the other methods while the Cut+CNN is only slightly better than the cut-based method. The situation is the same for all the other CNN architectures we have tested. The CNN is trained with more than 10^5 sample events that contain equal numbers of signal and background events. We monitor the training of the CNN by its accuracy on the training and valida-

tion sets with a classification threshold of 0.5. We have observed that the classification accuracy plateaus near 90% during the training, which signals the saturation of the CNN performance. However, increasing the classification threshold for the tested CNN does not improve the Higgs signal significance as sharply as that for the BDT or the FCNN, since the tested CNN assigns high scores for some background events just like for the signal events. As a result, the CNN gives the worst performance among the machine learning methods, and its training accuracy always collapses after going through several epochs even if we use smaller amount of training data. It is hard to decipher the CNN black box, and we only provide an educated guess for such an under-performance of the tested CNN as follows. Although the CNN is renowned for its ability to recognize shapes and edges in an image, it is not clear whether the CNN is equally good at perceiving precise numerical correlations over large separation in an image. The latter type of information such as the di-jet mass and missing mass are used directly as input variables of the BDT and FCNN. However, it may be hard for the CNN to recognize these variables because it takes several convolutions to correlate two far-separated points while the numerical precision might be lost during pooling. We thus conclude that the CNN architecture presented above is not a suitable ML technique for the Higgs preselection and leave a possible improvement of the performance to a future study.

Yukawa coupling measurements.— To showcase the importance of the improved preselection by the BDT and FCNN, we estimate the resultant improvement on sensitivities to the bottom, charm and strange Yukawa couplings measured or constrained by $H \rightarrow f\bar{f}$ (f is a quark) searches in the absence of systematic uncertainty. Assuming the SM value for the Higgs production cross section, the signal strength is given by

$$\mu_{ff} = \frac{\text{Br}(H \rightarrow f\bar{f})}{\text{Br}^{\text{SM}}(H \rightarrow f\bar{f})}. \quad (5)$$

Here, $\text{Br}^{\text{SM}}(H \rightarrow f\bar{f})$ denotes the SM expectation of the branching ratio for $H \rightarrow f\bar{f}$. We now define the number of events that pass the preselection of $H \rightarrow jj$ and the subsequent quark flavor tagging as $N_f = S_f + B_f$ where S_f (B_f) is the number of signal (background) events. They are related to their SM expectation values via $S_f \simeq \mu_{ff} S_f^{\text{SM}}$ and $B_f \simeq B_f^{\text{SM}}$. The statistical

² With the neural networks discussed in this work, the background is solely estimated from their performance on the simulation data. A practical bump search usually performs a sideband fit for better control of background estimation and systematic uncertainties. The combination of the NNs and the sideband subtraction method will require additional treatment[45–51] to decouple the NN from resonance-sensitive variables such as the invariant mass.

significance of deviation from the SM is characterized by

$$\chi^2 \equiv \frac{(N_f - N_f^{\text{SM}})^2}{N_f^{\text{SM}}} \simeq \left(\frac{(\mu_{ff} - 1)S_f^{\text{SM}}}{\sqrt{S_f^{\text{SM}} + B_f^{\text{SM}}}} \right)^2, \quad (6)$$

where $\chi \simeq 1$ (1.96) corresponds to the 1σ (95% C.L.) deviation. Since the bottom and charm Yukawa couplings are expected to be measured at future lepton colliders, we assume that both the true and observed central values are $\mu_{ff} = 1$ ($f = b, c$) and estimate the 1σ errors by requiring $\chi < 1$. On the other hand, for the strange Yukawa coupling, we obtain the 95% C.L. upper bound on μ_{ss} by requiring $\chi < 1.96$.

For the bottom and charm quark tagging, we assume a set of tagging efficiencies presented in a CEPC study [52] where an inclusive $Z \rightarrow q\bar{q}$ sample is used.³ The b -jet tagging efficiency, mistagging rate of the c -jet and mistagging rate of the other light quark or gluon jet are $\epsilon_b = 80\%$, $\epsilon_c^{\text{bkg}} = 8\%$ and $\epsilon_q^{\text{bkg}} = 1\%$, respectively. Similarly, the c -jet tagging efficiency, mistagging rate of the b -jet and mistagging rate of the other light quark or gluon jet are $\epsilon_c = 60\%$, $\epsilon_b^{\text{bkg}} = 14\%$ and $\epsilon_q^{\text{bkg}} = 7\%$, respectively. The strange jet tagging is much less efficient. For a rough estimate, we adopt the tagging method presented in ref. [20] where the efficiency of tagging two signal s -jets, mis-tagging rate of two background jets from a $H \rightarrow jj$ process and mis-tagging rate of two jets from a non- $H \rightarrow jj$ process are $\epsilon_{ss} = 96\%$, $\epsilon_{\text{bkg}}^{H \rightarrow jj} = 26\%$ and $\epsilon_{\text{bkg}}^{\text{non-}jj} = 70\%$, respectively.

In table IV, we summarize the expected 1σ errors of the signal strength for the bottom and charm quarks and the 95% C.L. upper limits on that of the strange quark with various preselection methods according to the performances listed in Table III, assuming only statistical uncertainty. For a conservative estimate, we have assumed that a background event is counted in B_f^{SM} whenever it contains two jets that are tagged as the flavor of our concern. The table indicates that the cut-based method reaches a good precision of 2% for the bottom Yukawa, while the BDT and FCNN improve it marginally. The BDT and FCNN preselection methods give a similar measurement precision of μ_{cc} , roughly 16%, which improves significantly from the cut-based result of 34%. The precision is weakened in the combined analysis of the Cut+BDT or Cut+FCNN, which determines the signal strength μ_{cc} with a 21% or 22% error, respectively. We can see that the power of ML methods in reject-

ing backgrounds is essential for the charm-Yukawa precision measurement. For the strange Yukawa, the BDT and FCNN preselection methods result in 95% C.L. upper bounds, $\mu_{ss} \lesssim 36$ and $\mu_{ss} \lesssim 35$ respectively, which are again significantly better than the cut-based result of $\mu_{ss} \lesssim 70$.

We have shown that the ML methods can significantly reduce the statistical error in the charm and strange Yukawa measurements. On the other hand, the ignored systematic uncertainty, including those from the tagging efficiencies, event simulations and signal/background modeling have to be included in the limit setting. A further treatment of systematic uncertainty is important for the bottom and charm Yukawa measurements where statistical uncertainty is small, as shown in Table IV. For the strange Yukawa, the dominant uncertainty may still be statistical.

Conclusions.— We have studied how ML can help improve the performance for the preselection of $H \rightarrow jj$ events at future e^+e^- colliders. The BDT, FCNN and CNN were applied to select $H \rightarrow jj$ events from a large amount of backgrounds of ZZ , W^+W^- , $q\bar{q}$, $e^\pm\nu W^\mp$ and e^+e^-Z . Our result indicates that the FCNN performs the best in improving the Higgs signal significance and is significantly better than the cut-based method, while the BDT has a slightly weaker but comparable capability. On the contrary, the CNN we have used is not suitable for the Higgs preselection task, and the result of CNN is suboptimal. The performance is not improved even if we take less or more training data. We also tested the performance of combinations of the ML methods with the cut-based selection. Such combinations degrade the resulting signal significance of the BDT and FCNN since only a limited number of signal events pass the cut-based selection. Nevertheless, the combined methods may be useful if one needs strict control of probable background events.

The precision measurement of the quark Yukawa couplings is one of the most important missions at future lepton collider experiments. The Higgs preselection based on the BDT and FCNN algorithms improves sensitivities to the charm and strange Yukawa couplings significantly compared to the conventional cut-based analysis, while only a mild improvement has been observed for the bottom Yukawa coupling. In summary, the BDT and FCNN algorithms are highly useful to select $H \rightarrow jj$ events and improve direct measurements on the light quark Yukawa couplings at future lepton colliders.

ACKNOWLEDGEMENTS

We would like to thank Gang Li, Kun Liu, Hiroaki Ono, Manqi Ruan, Junfeng Wu and Dan Yu for the discussions. SC was supported by JSPS KAKENHI Grant No. 20J00046. SC was supported by the Director, Of-

³ For simplicity, we assume that the tagging efficiencies for $H \rightarrow q\bar{q}$ events are comparable to those of ref. [52]. The purpose of our analysis is to compare the performance of various machine learning approaches to the Yukawa coupling measurements, and a more rigorous treatment of the flavor tagging is beyond the scope of the current paper.

Office of Science, Office of High Energy Physics of the U.S. Department of Energy under the Contract No. DE-AC02-05CH1123. YN is supported by Natural Science Foundation of China under grant No. 12150610465.

-
- [1] **ATLAS** Collaboration, G. Aad *et al.*, “Observation of a new particle in the search for the Standard Model Higgs boson with the ATLAS detector at the LHC,” *Phys. Lett. B* **716** (2012) 1–29, [arXiv:1207.7214 \[hep-ex\]](#).
- [2] **CMS** Collaboration, S. Chatrchyan *et al.*, “Observation of a New Boson at a Mass of 125 GeV with the CMS Experiment at the LHC,” *Phys. Lett. B* **716** (2012) 30–61, [arXiv:1207.7235 \[hep-ex\]](#).
- [3] **ATLAS** Collaboration, M. Aaboud *et al.*, “Observation of $H \rightarrow b\bar{b}$ decays and VH production with the ATLAS detector,” *Phys. Lett. B* **786** (2018) 59–86, [arXiv:1808.08238 \[hep-ex\]](#).
- [4] **CMS** Collaboration, A. M. Sirunyan *et al.*, “Observation of Higgs boson decay to bottom quarks,” *Phys. Rev. Lett.* **121** no. 12, (2018) 121801, [arXiv:1808.08242 \[hep-ex\]](#).
- [5] **CMS** Collaboration, A. M. Sirunyan *et al.*, “A search for the standard model Higgs boson decaying to charm quarks,” *JHEP* **03** (2020) 131, [arXiv:1912.01662 \[hep-ex\]](#).
- [6] **ATLAS** Collaboration, “Direct constraint on the Higgs-charm coupling from a search for Higgs boson decays to charm quarks with the ATLAS detector,”.
- [7] **ATLAS** Collaboration, M. Aaboud *et al.*, “Searches for exclusive Higgs and Z boson decays into $J/\psi\gamma$, $\psi(2S)\gamma$, and $\Upsilon(nS)\gamma$ at $\sqrt{s} = 13$ TeV with the ATLAS detector,” *Phys. Lett. B* **786** (2018) 134–155, [arXiv:1807.00802 \[hep-ex\]](#).
- [8] J. Gao, “Probing light-quark Yukawa couplings via hadronic event shapes at lepton colliders,” *JHEP* **01** (2018) 038, [arXiv:1608.01746 \[hep-ph\]](#).
- [9] A. L. Kagan, G. Perez, F. Petriello, Y. Soreq, S. Stoynev, and J. Zupan, “Exclusive window onto higgs yukawa couplings,” *Physical Review Letters* **114** no. 10, (Mar, 2015) . <http://dx.doi.org/10.1103/PhysRevLett.114.101802>.
- [10] M. König and M. Neubert, “Exclusive radiative higgs decays as probes of light-quark yukawa couplings,” *Journal of High Energy Physics* **2015** no. 8, (Aug, 2015) . [http://dx.doi.org/10.1007/JHEP08\(2015\)012](http://dx.doi.org/10.1007/JHEP08(2015)012).
- [11] G. Perez, Y. Soreq, E. Stamou, and K. Tobioka, “Prospects for measuring the higgs boson coupling to light quarks,” *Physical Review D* **93** no. 1, (Jan, 2016) . <http://dx.doi.org/10.1103/PhysRevD.93.013001>.
- [12] **ATLAS** Collaboration, M. Aaboud *et al.*, “Search for exclusive Higgs and Z boson decays to $\phi\gamma$ and $\rho\gamma$ with the ATLAS detector,” *JHEP* **07** (2018) 127, [arXiv:1712.02758 \[hep-ex\]](#).
- [13] **CEPC Study Group** Collaboration, M. Dong *et al.*, “CEPC Conceptual Design Report: Volume 2 - Physics & Detector,” [arXiv:1811.10545 \[hep-ex\]](#).
- [14] A. Blondel, J. Gluza, S. Jadach, P. Janot, and T. Riemann, eds., *Theory for the FCC-ee: Report on the 11th FCC-ee Workshop Theory and Experiments*, vol. 3/2020 of *CERN Yellow Reports: Monographs*. CERN, Geneva, 5, 2019. [arXiv:1905.05078 \[hep-ph\]](#).
- [15] **ILC** Collaboration, G. Aarons *et al.*, “ILC Reference Design Report Volume 1 - Executive Summary,” [arXiv:0712.1950 \[physics.acc-ph\]](#).
- [16] **ATLAS** Collaboration, G. Aad *et al.*, “Performance of b -Jet Identification in the ATLAS Experiment,” *JINST* **11** no. 04, (2016) P04008, [arXiv:1512.01094 \[hep-ex\]](#).
- [17] **CMS** Collaboration, A. M. Sirunyan *et al.*, “Identification of heavy-flavour jets with the CMS detector in pp collisions at 13 TeV,” *JINST* **13** no. 05, (2018) P05011, [arXiv:1712.07158 \[physics.ins-det\]](#).
- [18] Y. Nakai, D. Shih, and S. Thomas, “Strange Jet Tagging,” [arXiv:2003.09517 \[hep-ph\]](#).
- [19] J. Erdmann, O. Nackenhorst, and S. V. Zeißner, “Maximum performance of strange-jet tagging at hadron colliders,” *JINST* **16** no. 08, (2021) P08039, [arXiv:2011.10736 \[hep-ex\]](#).
- [20] J. Duarte-Campderros, G. Perez, M. Schlaffer, and A. Soffer, “Probing the Higgs–strange-quark coupling at e^+e^- colliders using light-jet flavor tagging,” *Phys. Rev. D* **101** no. 11, (2020) 115005, [arXiv:1811.09636 \[hep-ph\]](#).
- [21] A. J. Larkoski, I. Mould, and B. Nachman, “Jet Substructure at the Large Hadron Collider: A Review of Recent Advances in Theory and Machine Learning,” *Phys. Rept.* **841** (2020) 1–63, [arXiv:1709.04464 \[hep-ph\]](#).
- [22] Y.-L. Chung, S.-C. Hsu, and B. Nachman, “Disentangling Boosted Higgs Boson Production Modes with Machine Learning,” [arXiv:2009.05930 \[hep-ph\]](#).
- [23] J. Lin, M. Freytsis, I. Mould, and B. Nachman, “Boosting $H \rightarrow b\bar{b}$ with Machine Learning,” *JHEP* **10** (2018) 101, [arXiv:1807.10768 \[hep-ph\]](#).
- [24] R. Santos, M. Nguyen, J. Webster, S. Ryu, J. Adelman, S. Chekanov, and J. Zhou, “Machine learning techniques in searches for $t\bar{t}h$ in the $h \rightarrow b\bar{b}$ decay channel,” *JINST* **12** no. 04, (2017) P04014, [arXiv:1610.03088 \[hep-ex\]](#).
- [25] H. Ono and A. Miyamoto, “A study of measurement precision of the Higgs boson branching ratios at the International Linear Collider,” *Eur. Phys. J. C* **73** no. 3, (2013) 2343, [arXiv:1207.0300 \[hep-ex\]](#).
- [26] Y. Bai, “ $h \rightarrow bb/cc/gg$ branch ratio measurement in cpc.” 3rd cpc physics software meeting, 2016. <http://indico.ihep.ac.cn/event/6495/session/1/contribution/6/material/slides/0.pdf>.
- [27] H. Abramowicz, A. Abusleme, K. Afanaciev, N. Alipour Tehrani, C. Balázs, Y. Benhammou, M. Benoit, B. Bilki, J.-J. Blaising, M. J. Boland, and et al., “Higgs physics at the clic electron–positron linear collider,” *The European Physical Journal C* **77** no. 7, (Jul, 2017) . <http://dx.doi.org/10.1140/epjc/s10052-017-4968-5>.
- [28] J. Alwall, R. Frederix, S. Frixione, V. Hirschi, F. Maltoni, O. Mattelaer, H. S. Shao, T. Stelzer, P. Torrielli, and M. Zaro, “The automated computation of tree-level and next-to-leading order differential cross sections, and their matching to parton shower simulations,” *JHEP* **07** (2014) 079, [arXiv:1405.0301 \[hep-ph\]](#).
- [29] T. Sjostrand, S. Mrenna, and P. Z. Skands, “PYTHIA 6.4 Physics and Manual,” *JHEP* **05** (2006) 026, [arXiv:hep-ph/0603175](#).

- [30] T. Sjöstrand, S. Ask, J. R. Christiansen, R. Corke, N. Desai, P. Ilten, S. Mrenna, S. Prestel, C. O. Rasmussen, and P. Z. Skands, “An introduction to PYTHIA 8.2,” *Comput. Phys. Commun.* **191** (2015) 159–177, [arXiv:1410.3012 \[hep-ph\]](#).
- [31] **DELPHES 3** Collaboration, J. de Favereau, C. Delaere, P. Demin, A. Giammanco, V. Lemaître, A. Mertens, and M. Selvaggi, “DELPHES 3, A modular framework for fast simulation of a generic collider experiment,” *JHEP* **02** (2014) 057, [arXiv:1307.6346 \[hep-ex\]](#).
- [32] M. Cacciari, G. P. Salam, and G. Soyez, “FastJet User Manual,” *Eur. Phys. J. C* **72** (2012) 1896, [arXiv:1111.6097 \[hep-ph\]](#).
- [33] S. Catani, Y. L. Dokshitzer, M. Olsson, G. Turnock, and B. R. Webber, “New clustering algorithm for multi-jet cross-sections in e^+e^- annihilation,” *Phys. Lett. B* **269** (1991) 432–438.
- [34] S. Catani, Y. L. Dokshitzer, M. H. Seymour, and B. R. Webber, “Longitudinally invariant K_t clustering algorithms for hadron hadron collisions,” *Nucl. Phys. B* **406** (1993) 187–224.
- [35] S. D. Ellis and D. E. Soper, “Successive combination jet algorithm for hadron collisions,” *Phys. Rev. D* **48** (1993) 3160–3166, [arXiv:hep-ph/9305266](#).
- [36] **CMS Collaboration** Collaboration, “A Cambridge-Aachen (C-A) based Jet Algorithm for boosted top-jet tagging,” tech. rep., CERN, Geneva, Jul, 2009. <https://cds.cern.ch/record/1194489>.
- [37] F. Pedregosa, G. Varoquaux, A. Gramfort, V. Michel, B. Thirion, O. Grisel, M. Blondel, P. Prettenhofer, R. Weiss, V. Dubourg, J. VanderPlas, A. Passos, D. Cournapeau, M. Brucher, M. Perrot, and E. Duchesnay, “Scikit-learn: Machine learning in python,” *CoRR* [abs/1201.0490](#) (2012) , 1201.0490. <http://arxiv.org/abs/1201.0490>.
- [38] J. Z. H. Z. T. Hastie, S. Rosset, “Multi-class adaboost,” *Statistics and Its Interface* **2** no. 3, (2009) 349 – 360.
- [39] B. van Merriënboer, D. Bahdanau, V. Dumoulin, D. Serdyuk, D. Warde-Farley, J. Chorowski, and Y. Bengio, “Blocks and fuel: Frameworks for deep learning,” *CoRR* [abs/1506.00619](#) (2015) , 1506.00619. <http://arxiv.org/abs/1506.00619>.
- [40] M. Abadi, P. Barham, J. Chen, Z. Chen, A. Davis, J. Dean, M. Devin, S. Ghemawat, G. Irving, M. Isard, *et al.*, “Tensorflow: A system for large-scale machine learning,” in *12th {USENIX} Symposium on Operating Systems Design and Implementation ({OSDI} 16)*, pp. 265–283. 2016.
- [41] “Multilayer feedforward networks are universal approximators,” *Neural Networks* **2** (1989) 359–366.
- [42] P. T. Komiske, E. M. Metodiev, and M. D. Schwartz, “Deep learning in color: towards automated quark/gluon jet discrimination,” *JHEP* **01** (2017) 110, [arXiv:1612.01551 \[hep-ph\]](#).
- [43] M. Cacciari, G. P. Salam, and G. Soyez, “The anti- k_t jet clustering algorithm,” *JHEP* **04** (2008) 063, [arXiv:0802.1189 \[hep-ph\]](#).
- [44] M. D. Zeiler, “ADADELTA: an adaptive learning rate method,” *CoRR* [abs/1212.5701](#) (2012) , 1212.5701. <http://arxiv.org/abs/1212.5701>.
- [45] C. Englert, P. Galler, P. Harris, and M. Spannowsky, “Machine Learning Uncertainties with Adversarial Neural Networks,” *Eur. Phys. J. C* **79** no. 1, (2019) 4, [arXiv:1807.08763 \[hep-ph\]](#).
- [46] S. Wunsch, S. Jörger, R. Wolf, and G. Quast, “Reducing the dependence of the neural network function to systematic uncertainties in the input space,” *Comput. Softw. Big Sci.* **4** no. 1, (2020) 5, [arXiv:1907.11674 \[physics.data-an\]](#).
- [47] L. Bradshaw, R. K. Mishra, A. Mitridate, and B. Ostdiek, “Mass Agnostic Jet Taggers,” *SciPost Phys.* **8** no. 1, (2020) 011, [arXiv:1908.08959 \[hep-ph\]](#).
- [48] G. Kasieczka and D. Shih, “Robust Jet Classifiers through Distance Correlation,” *Phys. Rev. Lett.* **125** no. 12, (2020) 122001, [arXiv:2001.05310 \[hep-ph\]](#).
- [49] K. Benkendorfer, L. L. Pottier, and B. Nachman, “Simulation-assisted decorrelation for resonant anomaly detection,” *Phys. Rev. D* **104** no. 3, (2021) 035003, [arXiv:2009.02205 \[hep-ph\]](#).
- [50] O. Kitouni, B. Nachman, C. Weisser, and M. Williams, “Enhancing searches for resonances with machine learning and moment decomposition,” *JHEP* **21** (2020) 070, [arXiv:2010.09745 \[hep-ph\]](#).
- [51] A. Ghosh and B. Nachman, “A cautionary tale of decorrelating theory uncertainties,” *Eur. Phys. J. C* **82** no. 1, (2022) 46, [arXiv:2109.08159 \[hep-ph\]](#).
- [52] M. Ruan *et al.*, “Reconstruction of physics objects at the Circular Electron Positron Collider with Arbor,” *Eur. Phys. J. C* **78** no. 5, (2018) 426, [arXiv:1806.04879 \[hep-ex\]](#).